ACS OMEGA

Open Access

http://pubs.acs.org/journal/acsodf

Article

Mechanistic Insights into Plasma Oxidation of Ag Nanofilms: Experimental and Theoretical Studies

ChengCheng Yuan, Dan Zhang,* and Yang Gan*

Cite This: *ACS Omega* 2024, 9, 28912−28925

Read Online

ACCESS | Metrics & More | Article Recommendations | Supporting Information

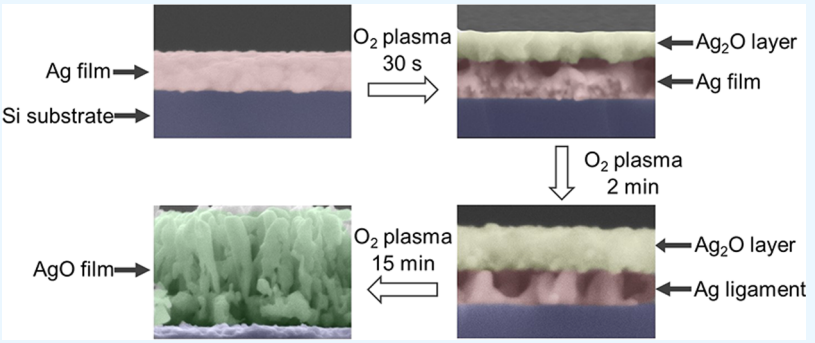

ABSTRACT: Plasma oxidation of metals has been studied extensively to fabricate nanoporous oxides with the merits of room temperature treatment and facile control of the oxidation rate. Plasma oxidation of Ag, motivated by studies on atomic oxygen corrosion of Ag, is one of the most studied systems. However, several important questions remain unaddressed and even overlooked traditionally: the critical role played by atomic O in promoting oxidation, evolution of microstructures during plasma exposure, and a sound framework for quantitative oxidation kinetic analyses. In this paper, the O_2 plasma oxidation behavior of Ag films deposited on Si substrates was systematically studied both experimentally and theoretically. The effects of plasma pressure and power on the microstructural evolution and oxidation kinetics of Ag films of various thicknesses were investigated using comprehensive characterization, as well as numerical analysis of plasma chemistry for deriving atomic O concentration. The findings here provide a full picture and deep mechanistic insights into the morphology and microstructure evolution of Ag films and the growth of dense or porous Ag_2O and AgO oxide layers by plasma oxidation, revealing the intricate interplay between atomic O, vacancy creation, Ag ion diffusion, Kirkendall effect, formation of pores, and interfacial void coalescence. The methodology developed here can be easily transferred to help understand the plasma oxidation behavior of other metals.

INTRODUCTION

Plasma oxidation of materials, in which samples are exposed to oxidative plasma (O_2, Ar/O_2, or air plasma), has been used extensively to fabricate oxides including NiO, Al_2O_3, SiO_2, Cu_2O/CuO, and Ag_2O/AgO.[1−7] Plasma oxidation exhibits advantages for fabricating oxides over other methods like thermal oxidation in that oxidation can be realized at rather low temperatures with a controlled rate by varying gas pressure and input power values. Studies about plasma oxidation of Ag were motivated by studying the atomic oxygen corrosion of Ag—as electron conductive materials or reflective media on solar concentrators in spacecraft—in the low earth orbit where abundant atomic oxygen species (they are also the reactive species in oxidative plasma) attack exposed surfaces.[8−11] In recent years, different silver oxide structures, such as Ag_2O nanotubes, Ag_2O/AgO porous films, and Ag_2O hollow nanoparticles, have been successfully fabricated by plasma oxidation.[12−17] These as-fabricated silver oxides and reduced Ag have been used as surface-enhanced Raman scattering substrates, photocatalysts, and electrode materials in supercapacitors and batteries.[17−20]

It is well recognized that the Ag material undergoes distinct compositional and microstructural changes during plasma oxidation, and the conversion of solid Ag to porous silver oxide occurs through the Kirkendall effect at the early stage and growth stress at the later stage.[13,16] It was Li et al. who, for the first time, confirmed the occurrence of the Kirkendall effect in the study of Ar/O_2 plasma oxidation of Ag nanowires.[16] They demonstrated that the Kirkendall effect was induced by faster outward diffusion of Ag ions. They observed, using transmission electron microscopy (TEM), generation of Kirkendall

Received: April 14, 2024
Revised: May 31, 2024
Accepted: June 5, 2024
Published: June 17, 2024

voids within the Ag_2O shell/Ag core interfacial region and conversion of Ag nanowires into Ag_2O nanotubes. However, fine microstructural features of oxidized Ag nanowires were not clearly resolved, and the surface chemical composition was not characterized. Moreover, the growth kinetics of oxide layers were not paid any attention. El Mel et al. extensively studied the plasma oxidation of the Ag material in various dimensions, including nanoparticles, nanocolumns, and Ag/Au films treated with air/oxygen plasma at 20/100 W.[12−14] They also demonstrated that plasma oxidation of Ag nanoparticles proceeded in three stages. Nevertheless, they failed to record the inner microstructural changes in Ag nanoparticles throughout the entire plasma process using TEM. A comprehensive characterization of both surface and bulk composition of oxidized samples was also lacking. Furthermore, the growth kinetics of the oxide layer was analyzed with a seemingly simple calculation of the diffusion coefficient of Ag ions based on Fick's first law; this can be problematic because sound mechanistic analyses into oxidation processes were not provided.

Xu et al. studied the oxidation of 300 nm thick Ag films during reactive sputtering deposition of NiO in an Ar/O_2 atmosphere at 100 W and 150 °C.[15,18−20] The oxidation process was revealed: first, a compact Ag_2O layer formed on the surface of a Ag film, then the compact Ag_2O film transformed into AgO nanorods, and finally nanopores formed within AgO nanorods. They attributed the formation of AgO nanorods and generation of nanopores to a special Kirkendall effect during the alloying of AgO and deposited NiO. Similarly, they proposed that oxide growth followed parabolic kinetics without deep mechanistic analyses into oxidation processes. Ma et al. treated a 600 nm thick Ag film with O_2 plasma at 25 W.[17] The Ag film was partially oxidized, forming a nanoporous Ag_2O/AgO film on the Ag film. They attributed the partial oxidation of thick Ag films to the limited penetration depth of the O_2 plasma without considering the main oxidation mechanism like outward diffusion of Ag ions. A close scrutiny of their scanning electron microscopy (SEM) images revealed that the oxide film is seriously wrinkled. Wang et al. treated thicker Ag films (1 μm) with Ar/O_2 plasma at 25−100 W to study the morphological changes.[2] Using SEM, they observed that Ag_2O films in a hillock morphology cracked into Ag_2O islands. Without complete characterization of Ag_2O/Ag interfacial microstructures, surface morphological changes were assumed to be induced by the Kirkendall effect and growth stress within the Ag_2O layer. Analyses of growth kinetics were lacking because the oxide thickness was not determined.

Critical evaluation of published results presented above revealed that it is difficult to gain a deeper mechanistic understanding of plasma oxidation of the Ag material without (1) a systematic characterization of the microstructural/compositional changes in the Ag material during plasma oxidation and (2) quantitative oxidation kinetic analyses based on the sound mechanistic understanding and measurements of time-related oxide film thickness, as well as (3) the very important yet seriously overlooked analyses of the concentration of atomic O in oxidative plasma, which are essential for a complete understanding of oxidation mechanism and oxidation kinetics. Only after these problems are addressed can a clear and full picture of the plasma oxidation of the Ag material be firmly established.

These problems cannot be satisfactorily addressed without careful choice of experimental systems, plasma conditions, systematic experiments/comprehensive characterization, and quantitative analyses/calculations. Ag films, with uniform and controlled thicknesses as well as homogeneous cross sections over large areas (square millimeters) for pristine films, are advantageous over Ag nanoparticles or nanowires in terms of facile characterization of morphologies/microstructures and determination of the thickness of oxide layers using top-view and side-view SEM and TEM. Low-power plasma is preferred over high-power conditions because of the slower oxidation process so that the full spectrum of surface morphology and microstructure evolution at different stages can be recorded. Although direct experimental measurements of the concentration of active atomic O in a plasma chamber cannot be realized in most laboratories, numerical calculations will greatly aid our understanding of the plasma power and pressure dependence of the concentration of atomic O.

In this paper, the O_2 plasma oxidation behavior of Ag films deposited on Si substrates is thoroughly studied both experimentally and theoretically. The effect of plasma pressure and power on microstructural evolution and oxidation kinetics of Ag films of various thicknesses is systematically investigated using comprehensive SEM, TEM, X-ray photoelectron spectroscopy (XPS), X-ray diffraction (XRD) characterization, and numerical calculation of the concentration of atomic O. The findings reported here contribute significantly to gaining insights into plasma oxidation of Ag and other metals.

EXPERIMENTAL SECTION

Wafer Cutting and Cleaning. Single-side-polished silicon wafers of 4 in. in diameter (LiJing Inc., China) were used as substrates for silver deposition. A Si wafer was cut into pieces before cleaning and Ag deposition by mechanical fracture treatment. The rough side of a Si wafer was scored using a diamond scriber, and then the wafer was pressed along the scoring mark to break it into desired pieces. The piece sizes for SEM, XRD, and XPS characterization were 0.5 cm × 2.0 cm, 1.5 cm × 1.5 cm, and 0.5 × 0.5 cm, respectively. Si pieces were cleaned with a routine RCA method: first, pieces were soaked in the SPM solution ($H_2SO_4 + H_2O_2$ 3:1) for 20 min at 80 °C, then rinsed with DI water, and blown dried under N_2 gas; second, pieces were soaked in the SC1 solution ($NH_3 + H_2O_2 + H_2O$ 1:1:5) for 20 min at 80 °C, then rinsed with DI water, and blown dried under N_2 gas; finally, pieces were soaked in the SC2 solution ($HCl + H_2O_2 + H_2O$ 1:1:5) for 20 min at 80 °C, then rinsed with DI water, and blown dried under N_2 gas.[21]

Deposition of Ag Films on Si substrates. Deposition of Ag films on the smooth side of cleaned Si pieces was carried out with ion sputtering of the Ag foil (99.99%, Ted Pella Inc.) using a sputter coater (Cressington Scientific Instruments Inc., U.K.) in an Ar (99.99% purity) gas atmosphere. The distance between the target and the Si substrate was ca. 4 cm. A 3 min presputtering step without substrates put inside was enforced to remove containments from the target. Then, Ag films were deposited on the cleaned Si substrates with a current of 20 mA and a working pressure of 0.06 mbar. The thickness of the Ag film was controlled by varying the sputtering time.

Plasma Oxidation of Ag Films. The samples with Ag films deposited on Si pieces were treated with O_2 plasma (99.99% purity) using a radiofrequency plasma generator (Harrick, PDC-32G-2). The working pressure in the chamber was controlled by a flow meter. After a pristine Ag film sample

https://doi.org/10.1021/acsomega.4c03608
ACS Omega 2024, 9, 28912−28925

was loaded into the chamber, the pressure was set to the desired value, and the plasma generator was switched on at a specified power for a defined time. The power of the plasma generator has three levels: 6.8, 10.5, and 18 W. The O_2 pressure was 0.25−1.0 Torr. For each treatment with the specific exposure time at different power and pressure values, a new pristine Ag film sample was loaded into the chamber. After the treatment, this sample was unloaded for the following characterization methods and analyses. The temperature of the substrate during plasma treatment was measured using temperature indicating labels (Thermax) with a range of 37−65 °C with a precision of 3 °C in the range of 37−49 °C and a precision of 5 °C in the range of 49−65 °C. The room temperature during testing was 25 °C. One piece of the label was attached to a blank Si piece and loaded into the chamber. After being treated for a prescribed exposure time under certain power and pressure, the label was unloaded, and the highest mark displayed on the label was recorded as the substrate temperature at this specific plasma condition (note that the temperature rise from 25 to 37 °C cannot be measured).

Structural and Compositional Characterization. The surface morphology and microstructure of pristine and oxidized Ag films were characterized by using an FE-SEM (Supra 55, Carl Zeiss, Germany). The specimens for cross-sectional SEM characterization were obtained by mechanical fracture treatment. The underside (the rough side) of a sample was scored using a diamond scriber, and then the sample was pressed along the scoring mark to break it to expose the internal cross sections.

The specimens for cross-sectional TEM characterization were prepared with an FIB system (FEI Strata 400S) equipped with an argon-milling device (Gatan 695). A protective carbon cap was deposited on the region of interest. An argon-milling device was then used for thinning of thin lamellae to 150 nm at 30 kV and then to 80 nm at 5 kV. The final specimen size was 5 μm × 3 μm × 80 nm. The cross-sectional TEM characterization was completed using an HRTEM (FEI Talos F200X) operating at 200 kV.

The surface chemical composition of films was characterized by X-ray photoelectron spectroscopy (Thermo Fisher Scientific Esca Xi+) equipped with an Al Kα X-ray source. The binding energy of the spectra was calibrated against that of the C 1s peak at 284.8 eV.

Grazing incidence X-ray diffraction (XRD) patterns of the films were recorded by using a Bruker D8 Advance diffractometer with Cu Ka radiation (40 kV/40 mA). The angle of incidence of the X-rays with respect to the sample surface was 5° to avoid interference of strong signals from underlying Si substrates.

The film thickness was analyzed with Image-Pro Plus 6.0 software (Media Cybernetics) based on cross-sectional SEM images. The average thickness values given in the paper were obtained by statistically analyzing at least 10 measurements. The film porosity was analyzed with AQUAMI (an open-source Python package)[22] based on the surface SEM images.

Calculation of the Concentration of Atomic O in O_2 Plasma. The highly nonlinear equations in the Supporting Information were optimally solved using the least-squares approach by leveraging commercially available software MATLAB or other open-source numerical simulation software. Specifically, the optimization was bound to ±30% relative to its initial values. It is worth noting that one may need several trials to determine the decent initial values and bounds for overcoming local optima.

RESULTS AND DISCUSSION

Typical O_2 plasma oxidation behavior of Ag films with different thicknesses (100−400 nm) was studied at a rather low plasma power (6.8 W) and 0.5 Torr (Figure 1). The division of film

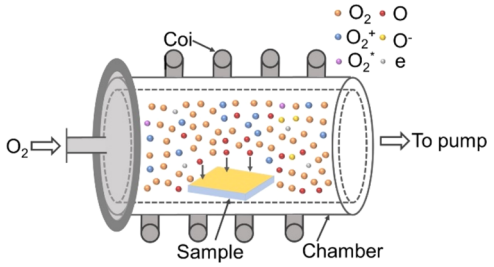

Figure 1. Schematic diagram of the induction plasma generator. O_2 was used as the working gas.

thickness into thinner and thicker regimes is based on the following observations: thinner Ag films (thickness <200 nm) show two-stage microstructural evolution and oxidation kinetics (change of oxide thickness over time); thus, studying this system is important for revealing the typical O_2 plasma oxidation of Ag films. Thicker films (thickness >200 nm) enable one to observe the more prominent evolution of interfacial microstructures for a partial oxidation system. The underlying reason that a universal critical thickness of around 200 nm exists is discussed from the diffusion-dominated void coalesce-induced interfacial detachment of the oxide layer from the underlying Ag film. The oxidation behavior was systematically investigated by using comprehensive SEM, XRD, XPS, and TEM characterization methods. Results for 200 nm thick Ag films treated at other pressures (0.25 Torr, 1.00 Torr) for 6.8 W and plasma power (10.5 W, 18 W) for 0.5 Torr are presented in the Supporting Information.

O_2 Plasma Oxidation of Thin Ag Films Showing Complete Two-Stage Oxidation Behavior. Top-view and side-view SEM images of 200 nm thick Ag films before and after O_2 plasma treatment for different times are presented in Figure 2a. It can be seen that both the surface morphology and microstructure of Ag films undergo significant changes during plasma oxidation. We need to emphasize that the results presented for each exposure time were obtained separately with a group of pristine Ag film samples prepared in a single Si wafer.

At the quite early stage of plasma oxidation as short as 10 s, an upper layer appears on the Ag film surface. (We will call this upper layer the oxide layer as the structure and composition characterization shows later.) The oxide grains with an average size of 30 nm are smaller than pristine Ag polycrystalline nanosized grains (average size of 70 nm obtained from the top-view image analysis). The average thickness of the upper layer is 75 nm, and that of the remaining Ag film is 145 nm. Small voids are present along the oxide/Ag interface. At an exposure time of 30 s, the oxide layer becomes thicker (120 nm), whereas the Ag film becomes thinner (115 nm), and voids enlarge. Bridges, connecting the oxide layer to the unoxidized Ag film, appear within the oxide/Ag interfacial region. Moreover, the side-view SEM image reveals that the voids are located largely within the Ag film. After being treated for 2

https://doi.org/10.1021/acsomega.4c03608
ACS Omega 2024, 9, 28912−28925

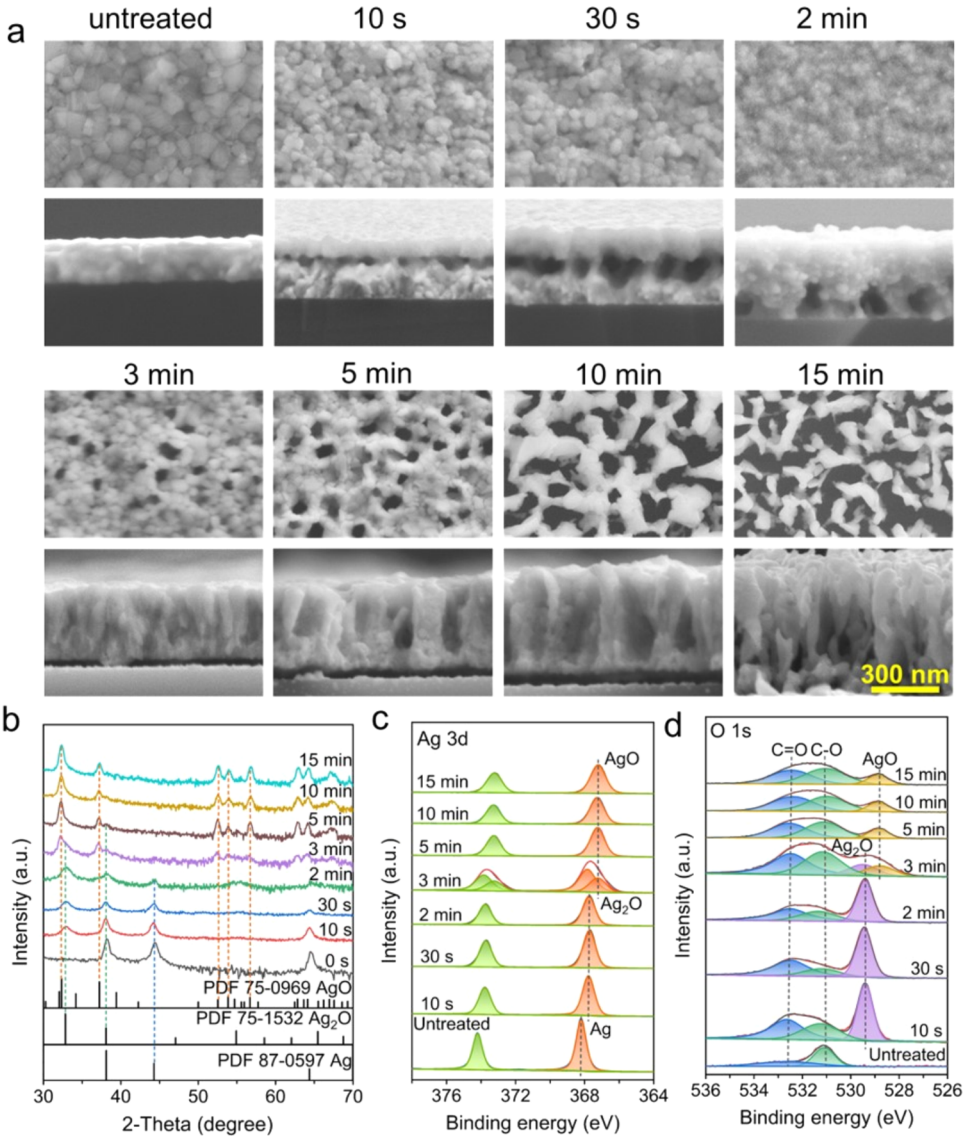

Figure 2. SEM images of 200 nm thick Ag films before and after O_2 plasma exposure for different times at 6.8 W, and the corresponding XPS spectra and XRD patterns. (a) Top-view and side-view SEM images. (b) XRD patterns, (c) Ag 3d XPS spectra, and (d) O 1s XPS spectra.

min, the thickness of the oxide layer further increases to 250 nm while the Ag film is nearly consumed; the bridges become more distinct with enlarged voids. Interestingly, the surface of the oxide layer seems to be free of voids within 2 min of treatment. Note that the adhesion between the film and the Si substrate within 2 min of treatment is strong because no cracking along the film and the Si substrate can be observed after SEM cross section specimen preparation.

After 3 min exposure, the bridges disappear, the Ag film is consumed, and pores appear on the surface of the oxide layer, as shown in the top-view SEM image (Figure 2a). For the case of 5 min, the side-view SEM image further reveals that the pores are across the oxide film. After being treated for 10 min, pores are found to be coalesced into larger pores with irregular shapes. The pore walls become thinner, as the side-view SEM image shows. At 15 min, the breaking of the ligaments between neighboring pores is observed. Note that both the thickness and pore size of the formed oxide film continuously increase with increasing time during the oxidation process until 15 min. The equivalent diameter of the pores, which is defined as the diameter of a circle with an equal sectional area, is quantified based on top-view SEM images. The equivalent diameter of the pores increases from 30 ± 8 nm at 3 min to 43 ± 10 nm at 5 min, to 77 ± 20 nm at 10 min, and to 90 ± 30 nm at 15 min. The film thickness increases from 320 ± 10 nm at 3 min, to 400 ± 15 nm at 5 min, to 520 ± 20 nm at 10 min, and to 615 ± 20 nm at 15 min. Then, the surface morphology, microstructure, and thickness of the oxide film remain unchanged even with prolonged treatment up to 20 min (results not shown). Note that the adhesion between the film and the Si substrate is not as good as those treated for shorter times; the cracking of the film from the Si substrate shown in several images in Figure 2a can be observed, which may be caused by mechanical fracture during the SEM cross section specimen preparation.

The XRD patterns of Ag films before and after O_2 plasma exposure for different times are presented in Figure 2b. All peaks of the untreated Ag film are indexed to Ag. Within 2 min, a peak at 32.8°, which is assigned to Ag_2O, appears and increases in intensity with time, whereas peaks of Ag decrease in intensity. At 3 min, several peaks at 32.3, 37.2, and 52.5° appear, and these peaks are identified as AgO; at the same

https://doi.org/10.1021/acsomega.4c03608
ACS Omega 2024, 9, 28912−28925

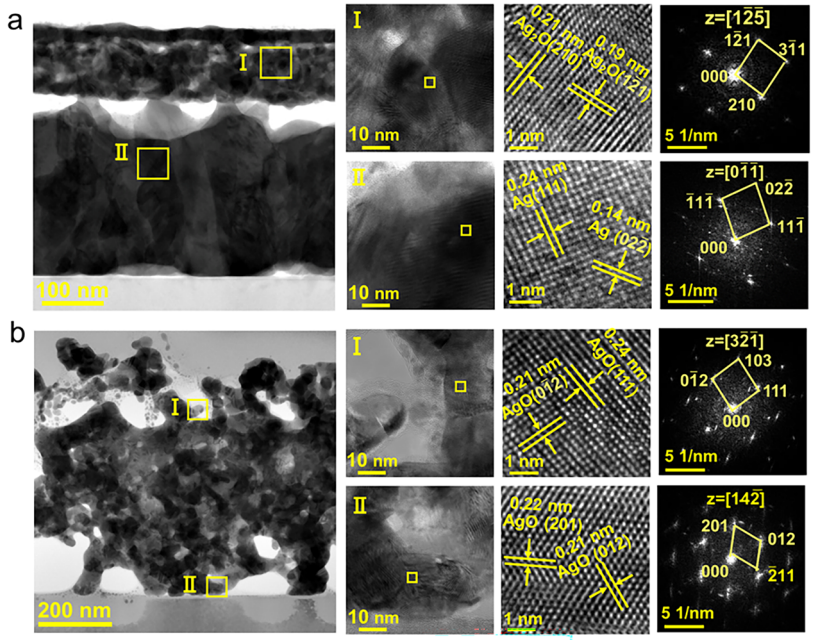

Figure 3. Cross-sectional TEM images, HRTEM images and corresponding FFT graphs of 200 nm thickness Ag films after O_2 plasma treatment for (a) 10 s and (b) 15 min. For the Ag film being treated for 10 s, HRTEM images of the regions of upper oxide layer (I) and lower Ag film (II) were analyzed. For the Ag film being treated for 15 min, HRTEM images of the top region (I) and bottom region (II) of the film were analyzed.

time, the peaks of Ag disappear. We argue that the disappearance of Ag peaks should be attributed to the consumption of the Ag film instead of the limited penetration depth of grazing X-ray (the penetration depth of the grazing X-ray exceeds 320 nm as discussed later for characterization of the thick oxide layer for the case of plasma oxidation of thick Ag films). It is thus evident that the Ag film was consumed after 3 min exposure; meanwhile, the $Ag_2O(111)$ peak at 32.8° and the $Ag_2O(200)$ peak at 38.1° are still present at 5 min but disappear at 15 min, indicating that Ag_2O is further oxidized to AgO.

Ag 3d and O 1s XPS spectra of Ag films before and after O_2 plasma exposure for different times are presented in Figure 2c,d. Ag $3d_{5/2}$ peaks broaden and shift from 368.2 eV (Ag) to 367.8 eV (Ag_2O) upon the exposure of O_2 plasma, indicating the growth of Ag_2O. At 3 min, there are two Ag $3d_{5/2}$ peaks at 367.8 eV (Ag_2O) and 367.3 eV (AgO). The peak at 367.8 eV (Ag_2O) disappears, and only the peak at 367.3 eV (AgO) is present after 5 min exposure, indicating that the outermost surface is further oxidized to AgO. The O 1s peak of untreated Ag films indicates the presence of adsorbed carbonaceous contamination on the Ag film. A shoulder peak located at 529.4 eV also indicates the growth of the Ag_2O layer. At 3 min, both Ag_2O and AgO (528.9 eV) peaks are observed. After 5 min exposure, the Ag_2O peak disappears. Changes in Ag 3d and O 1s peaks provide strong evidence of the initial formation of Ag_2O and the following transformation to AgO of the outermost surface of the oxide layer. Note that a slight decrease in the intensity of Ag 3d and O 1s peaks after 2 min exposure might be caused by pore generation and decreased area of the surface of the oxide layer. As reported, the number of signal electrons is affected by the surface topography of samples, and increased surface roughness could potentially decrease the signal intensity.[23,24]

Cross-sectional TEM images, HRTEM images, and corresponding FFT graphs of 200 nm thick Ag films after O_2 plasma exposure for 10 s and 15 min are presented in Figure 3. For the case of 10 s (Figure 3a), cross-sectional TEM images clearly show that the voids are located within the Ag film, and the bridges are a part of the Ag film. The average size of the Ag_2O grain is 20 nm (close to the value revealed by top-view SEM images) and is smaller than the underlying Ag grains. There are a few smaller voids in the upper part of the Ag_2O layer. The HRTEM images show that for the upper oxide layer, the lattice planes with spacings of 0.19 and 0.21 nm correspond to the (121) and (210) planes of crystalline Ag_2O, respectively; for the lower Ag film, the lattice planes with spacings of 0.24 and 0.14 nm correspond to the (111) and (022) planes of crystalline Ag, respectively. For the case of 15 min (Figure 3b), HRTEM images reveal that Ag has been completely oxidized to AgO. The average size of the AgO grain (35 nm) is larger than that of Ag_2O grains.

Results for Ag films of 200 nm thickness treated at other pressures (0.25 and 1.00 Torr) for 6.8 W and plasma power (10.5 and 18 W) for 0.5 Torr are presented in the Supporting Information. SEM images show that Ag films undergo similar changes in surface morphology and microstructure but at different oxidation rates (Figures S1 and S2). The plasma oxidation accelerates at higher power, and the Ag film is consumed at a treatment time of 30 s at 18 W. By contrast, plasma oxidation decelerates at higher pressure, and the Ag film is not consumed at a treatment time of 3 min at 1.0 Torr. Plasma oxidation of thinner 100 nm Ag films at different pressure/power values was also studied, showing similar changes in surface morphology and microstructure (results not shown), similar to 200 nm Ag films. We should point out that the substrate temperature rises during plasma treatment, and curves showing the temperature rises with time under different powers are given in Figure S3. The substrate temperatures treated at 6.8, 10.5, and 18 W for 15 min are 322, 327, and 333 K, respectively.

https://doi.org/10.1021/acsomega.4c03608
ACS Omega 2024, 9, 28912−28925

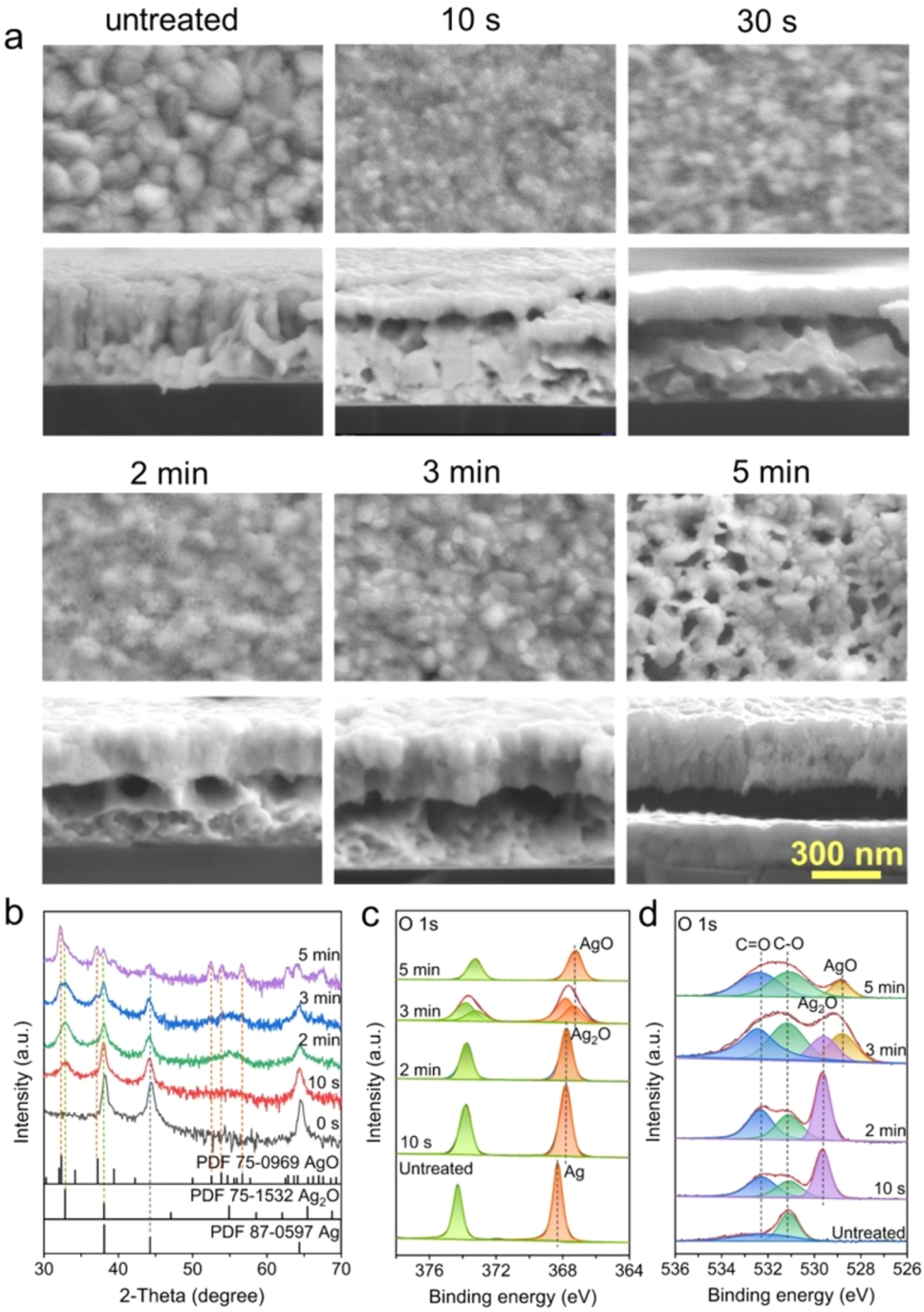

Figure 4. SEM images of 400 nm thick Ag films before and after O_2 plasma treatment for different times, and the corresponding XPS spectra and XRD patterns. (a) Top-view and side-view SEM images. (b) XRD patterns, (c) Ag 3d XPS spectra, and (d) O 1s XPS spectra.

Partial Oxidation of Thicker Ag Films Showing Prominent Evolution of Interfacial Microstructures and Detachment of Oxide Layer. In this section, a thicker Ag film with a thickness of 400 nm, treated with the same plasma power (6.8 W) and pressure (0.5 Torr) as above, showing the interesting partial oxidation behavior in O_2 plasma, will help reveal the evolution of interfacial microstructures between oxide layers and the underlying Ag film. This level of detailed evolution information cannot be obtained with a thin Ag film because of rather quick consumption of the underlying Ag film.

Top-view and side-view SEM images of 400 nm thick Ag films before and after O_2 plasma treatment for different times are presented in Figure 4a. The average size of the Ag grains is about 100 nm, and the grains are column-shaped along the film. At 10 s, a thin oxide layer grows on the Ag film, accompanied by the formation of voids along the oxide/Ag interface. The thickness is 80 nm for the oxide layer and 340 nm for the unoxidized Ag film. Compared with the pristine Ag grains, the oxide grains are smaller (30 nm). At 30 s, the oxide layer becomes thicker (125 nm), whereas the unoxidized Ag film becomes thinner (310 nm), and voids enlarge. After 2 min exposure, the thickness of the oxide layer reaches 220 nm, and the thickness of Ag films decreases to 230 nm. Then, the thickness of the unoxidized Ag film remains unchanged even with prolonged exposure, while the oxide layer continuously

https://doi.org/10.1021/acsomega.4c03608
ACS Omega 2024, 9, 28912−28925

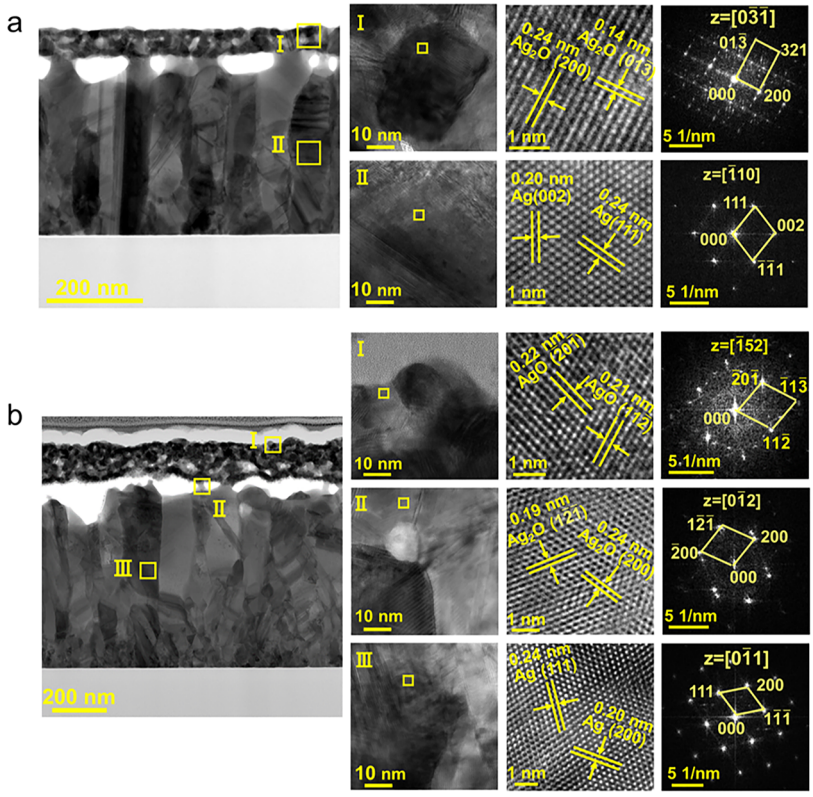

Figure 5. Cross-sectional TEM images, HRTEM images and corresponding FFT graphs of thick Ag films after O_2 plasma treatment for (a) 10 s (Ag film thickness: 400 nm) and (b) 2 min (Ag film thickness: 750 nm). For the Ag film being treated for 10 s, HRTEM images of the regions of upper oxide layer (I) and lower Ag film (II) were analyzed. For the Ag film being treated for 2 min, HRTEM images of the regions of upper oxide layer (I) , ligament (II) and lower Ag film (III) were analyzed.

thickens. At 5 min, the thickness of the oxide layer increases to 330 nm, pores are formed within the oxide layer, and a fissure separates the unoxidized Ag film from the oxide layer. Unlike the complete oxidation of 200 nm thick Ag films upon O_2 plasma exposure, only the upper part of the 400 nm thick Ag films is oxidized.

The XRD patterns of 400 nm thick Ag films before and after O_2 plasma oxidation for different times are presented in Figure 4b. All diffraction peaks of the untreated Ag film are indexed to Ag. Within 2 min, a peak at 32.8°, which is assigned to Ag_2O, appears and increases in intensity. After 3 min exposure, two peaks at 32.3 and 37.2°, which are assigned to AgO, appear and increase in intensity. The peaks of Ag can be observed even after 5 min of exposure, indicating that the penetration depth of the X-ray exceeds the thickness of the oxide layer (330 nm at 5 min). It should be noted that AgO is formed in the presence of remaining Ag; this finding is different from that of a thin Ag film, where AgO is formed only after underlying Ag is consumed.

The XPS spectra of 400 nm thick Ag films before and after O_2 plasma oxidation for different times are presented in Figure 4c,d. After initial exposure, the Ag $3d_{5/2}$ peak broadens and shifts from 368.2 eV (Ag) to 367.8 eV (Ag_2O). At 3 min, there are two Ag $3d_{5/2}$ peaks of Ag_2O and AgO, and the peak of Ag_2O disappears after treatment for 5 min. For the O 1s peak, a shoulder peak located at 529.4 eV (Ag_2O) appears after O_2 plasma exposure. At 3 min, both Ag_2O and AgO (528.9 eV) peaks were observed. After 5 min exposure, the Ag_2O peak disappears. It can thus be seen that 400 and 200 nm thick Ag films share similar changes in surface composition.

Cross-sectional TEM images, HRTEM images, and corresponding FFT graphs of thick Ag films after the O_2 plasma treatment for 10 s and 2 min are presented in Figure 5. For the case of 10 s (Figure 5a), an oxide layer is formed on the Ag film in a columnar morphology. The oxide grain is smaller than Ag grains. The average size of Ag_2O grains is 20 nm, while the Ag columns are 90 nm in width and 350 nm in length. The voids, with the shape of a plane upper part and curved lower part, are located within Ag films in the vicinity of the oxide/Ag interface, preferably at the grain boundaries. There are also a few smaller voids in the middle part of the Ag_2O layer. Analysis of the HRTEM images shows that for the upper oxide layer, the lattice planes with spacings of 0.24 and 0.14 nm correspond to the (200) and (013) planes of Ag_2O; for the Ag film, the lattice planes with spacings of 0.20 and 0.24 nm correspond to the (002) and (111) planes of Ag. Because the oxide layer after 2 min exposure for the sample of the 400 nm Ag film seriously flakes off during preparation of the TEM specimen, a thicker Ag film (750 nm) sample after the identical plasma oxidation treatment was employed for TEM characterization, as shown in Figure 5b. The average size of oxide grains is about 25 nm. Coalescence of voids and breaking of bridges can be observed. Analysis of the HRTEM images reveals that Ag_2O and AgO grains coexist in the oxide film.

Plasma oxidation of Ag films of 250 and 300 nm thickness treated at 0.5 Torr and 6.8 W was also studied (results not shown). Similar partial oxidation behavior as that of 400 nm Ag films was observed, i.e., coalescence of interfacial voids as oxidation proceeds until the breaking of bridges occurs and the oxide layer detaches from the remaining Ag film. Thickness

https://doi.org/10.1021/acsomega.4c03608
ACS Omega 2024, 9, 28912−28925

analyses reveal that a rather constant thickness (110−150 nm) of Ag is converted to an oxide layer before detachment occurs for these thicker Ag films.

Reconsidering the Critical Role of Atomic O in Plasma Oxidation of Ag Films: Plasma Power and Pressure Dependence of the Concentration of Atomic O. It is well recognized that atomic O is the most active species that is responsible for plasma oxidation of materials including Ag. An oxidative plasma environment provides active oxidizing species. O_2 plasma contains different types of oxygen species, including molecules (O_2), ions (O_2^+, O^-), metastable species (O_2*), and neutral free radicals (O), due to the electron-neutral reactions, such as ionization, dissociation, excitation, etc.[25−27] The concentration of the ions is much lower than that of neutrals. Atomic O is the most abundant except for neutral oxygen molecules in O_2 plasma.[4,28]

It is noteworthy that plasma chemists have already developed experimental and calculation tools for determining the atomic O concentration in the plasma atmosphere including O_2 and other gas mixtures.[25−27] Generally, the concentration of atomic O of O_2 plasma increases with power.[29] Regarding the pressure dependence of the concentration of atomic O, an intricate "volcano curve" behavior has been found.[30]

However, to our surprise, researchers studying plasma oxidation of materials have not paid much attention to the theoretical analyses of power and pressure dependence of the concentration of atomic O. Without these theoretical insights, a complete understanding of the oxidation mechanism and oxidation kinetics can hardly be gained. Although direct experimental measurements of the concentration of active atomic O in a plasma chamber cannot be realized in most laboratories, we see below that numerical calculation greatly aids our understanding of plasma power and pressure dependence of the oxidation rate.

Here, the concentration of atomic O at different pressure/power values was numerically calculated based on the established model of reaction kinetics in an O_2 plasma environment.[25−27] A multidimensional nonlinear set of algebraic equations is established based on charge neutrality, particle balance, and power balance (more details are given in the Supporting Information). Then, the concentration of atomic O can be obtained in the concerned power (6.8−18 W) and pressure ranges (0.25−1.00 Torr).

Calculation results show that the concentration of atomic O increases with power but decreases with pressure. At a fixed power of 6.8 W, the concentration of atomic O decreases with pressure from 5.0×10^{14} cm^{-3} at 0.25 Torr to 3.6×10^{14} cm^{-3} at 0.5 Torr and to 2.2×10^{14} cm^{-3} at 1.00 Torr. At a fixed pressure of 0.5 Torr, the concentration of atomic O increases with power from 3.6×10^{14} cm^{-3} at 6.8 W to 6.0×10^{14} cm^{-3} at 10.5 W and to 9.4×10^{14} cm^{-3} at 18 W. These results agree in the scale of magnitude and trends with other literature plasma kinetics results if evaluated at similar power and pressure levels.[27,29]

So, it is clear that there are a large number of dissociated atomic O species in the plasma chamber during plasma oxidation of Ag. Moreover, sticking coefficients of 0.9 and larger have been reported for atomic O on Ag.[31] In comparison, for conventional molecular oxygen oxidation, the dissociative sticking probability of atomic O from O_2 on the Ag surface at room temperature is as low as 10^{-6}−10^{-4}.[32] Furthermore, the sticking probability of atomic O on the oxide surface is also higher than that of atomic O from O_2.[33] It was reported that the thickness of the Ag oxide layer formed in ambient dry air is only about 1 nm.[34,35] Therefore, a markedly increased oxidation rate can thus be expected for the plasma oxidation of Ag.

In the following sections, we will see that obtained plasma power and pressure dependence of atomic O concentration will greatly help gain insights into not only enhanced plasma oxidation of Ag near room temperature but also plasma power and pressure dependence of the oxidation rate.

Without the presence of atomic O in a reactive environment like O_2 plasma, oxidation of Ag at dry ambient room temperature is very slow and negligible.[34] It has been reported that upon exposure of Ag to atomic O, Ag readily reacts with atomic O even at room temperature.[8] Atomic O chemisorption and oxide nucleation occur at the Ag surface, and several monolayers of Ag oxide are thus formed.[36]

Therefore, to our surprise, the critical role of atomic O in promoting O_2 plasma oxidation of Ag near room temperature has not been mechanistically understood from the perspective of the interaction between atomic O and initial Ag oxide. Researchers working on plasma oxidation of metals appreciated enhanced oxidation due to active atomic O, and outward diffusion of metal is much faster than inward diffusion of O, including Ag.[13,16,37−40] Outward diffusion of Ag ions is the dominant transport process in the growing Ag_2O layer film, and the oxide/gas interface is the reaction front. However, the detailed diffusion mechanism of Ag ions through the oxide layer was not clarified: it is well known that Ag vacancies are predominant defects in Ag_2O,[41] but the role of Ag vacancies in mediating the diffusion mechanism of Ag ions has not been established for the plasma oxidation of Ag, and how Ag vacancies are created at the Ag oxide surface at the presence of atomic O during plasma oxidation is unclear.

Aided with an early report,[41] the mechanism of creation of Ag vacancies on the surface of thin Ag oxide described above and the growing Ag oxide layer (Ag_2O, AgO) during plasma oxidation can be described as follows

$$O(g) \rightarrow Ag_2O + 2V'_{Ag} + 2h^{\bullet} \quad (1)$$

$$O(g) \rightarrow AgO + V''_{Ag} + 2h^{\bullet} \quad (2)$$

The corresponding mass action constant is as follows

$$K_1 = [V'_{Ag}]^2[h^{\bullet}]^2/a(O) \quad (3)$$

$$K_2 = [V''_{Ag}][h^{\bullet}]^2/a(O) \quad (4)$$

where square brackets denote the concentration in mole fractions (the number of defects per Ag_2O or AgO formula unit), and $a(O)$ is the activity of atomic oxygen. To maintain electric neutrality,

$$[V'_{Ag}] = [h^{\bullet}] \quad (5)$$

$$[V''_{Ag}] = 2[h^{\bullet}] \quad (6)$$

and thus,

$$[V'_{Ag}] \propto a(O)^{1/4} \quad (7)$$

$$[V''_{Ag}] \propto a(O)^{1/3} \quad (8)$$

https://doi.org/10.1021/acsomega.4c03608
ACS Omega 2024, 9, 28912−28925

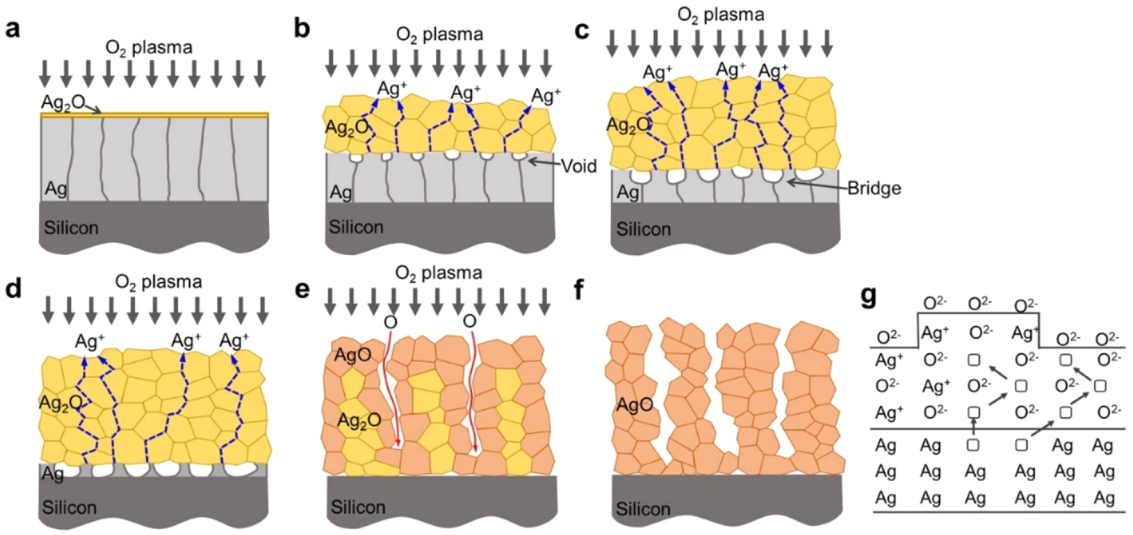

Figure 6. Schematic of the microstructural changes in thick Ag films during the O_2 plasma treatment (a–f) and outward diffusion of Ag ions through Ag vacancies (g).

indicating that the concentration of Ag vacancies at the Ag oxide depends on the concentration of atomic O. Moreover, because the activity of atomic oxygen is different at the surface of Ag oxide exposed to atomic O and the Ag oxide/Ag interface or Ag_2O/AgO interface ($a(O) = 0$ at both interfaces), a concentration gradient of Ag vacancies is thus established across the growing oxide layer.

According to Fick's diffusion law, the flux of Ag ions toward the Ag oxide surface is thus related to the concentration gradient of Ag vacancies and the diffusion coefficient of Ag ions in oxide layers

$$J_1 = -D_{Ag^+}[V'_{Ag}]/X_1 \quad (9)$$

$$J_2 = -D_{Ag^{2+}}[V''_{Ag}]/X_2 \quad (10)$$

where X_1 is the thickness of Ag_2O and X_2 is that of the AgO layer. Finally, from parts (7) and (8),

$$J_1 \propto -D_{Ag^+}a(O)^{1/4}/X_1 \quad (11)$$

$$J_2 \propto -D_{Ag^{2+}}a(O)^{1/3}/X_2 \quad (12)$$

Consequently, a few inspiring conclusions can be drawn from the analysis above.

(1) Because Ag vacancies are predominant defects in Ag_2O and AgO, upon exposure to atomic O, continuous creation of Ag vacancies occurs at the surface of Ag oxide, and a high concentration gradient of Ag vacancies is established between the surface of Ag oxide and the Ag oxide/Ag interface or Ag_2O/AgO interface. The critical role of atomic O in promoting O_2 plasma oxidation of Ag and Ag_2O near room temperature is thus mechanistically understood.

(2) It is also clear from (11) and (12) that the plasma oxidation rate is higher with larger $a(O)$. Because $a(O)$ depends on plasma power and pressure, it is thus not unexpected that one can observe plasma power and pressure dependence of the oxidation rate.

Mechanism of Morphology and Microstructure Evolution of Plasma Oxidation of Ag Films——Interplay among Atomic O, Ag Ion Diffusion, Kirkendall Effect, and Self-Limited Growth of Oxide Regulated by Interfacial Void Coalescence. In this section, the mechanism of morphology and microstructure evolution at different stages of plasma oxidation of Ag films in the O_2 plasma will be discussed. The intricate interplay among atomic O, Ag ion diffusion across Ag oxide, and the classical Kirkendall effect will be revealed for the first and second stages of oxidation for both thin and thick films, and for thick films, the self-limited growth of Ag oxide regulated by interfacial void coalescence will be discussed to explain the phenomenon that a rather constant thickness (110–150 nm) of Ag is converted to an oxide layer before the detachment of the oxide layer occurs.

For thin Ag films, two distinct oxidation stages can be distinguished: the first stage is oxidation of the Ag film to Ag_2O, and the second stage is conversion of Ag_2O to AgO. Figure 6 illustrates the complete process of oxidation.

(i) The first stage begins with formation of very thin oxide upon initial exposure to O_2 plasma (Figure 6a). Upon exposure of Ag to atomic O, Ag readily reacts with atomic O even at room temperature[8] because atomic O chemisorption and oxide nucleation occur at the Ag surface, and several monolayers of Ag oxide can be formed.[36] Because this layer is very thin and may form in less than 1 s, it is very challenging to measure its thickness via microscopic methods.

(ii) The gradient of Ag vacancy-mediated outward diffusion of Ag ions from Ag/Ag_2O to the surface of Ag_2O induced the growth of the Ag_2O film, and the nanoscale Kirkendall effect induced the formation and growth of interfacial voids (Figure 6b,c). As discussed in the last section, continuous creation of Ag vacancies occurs at the surface of Ag oxide during plasma exposure (eq 1), and a high concentration gradient of Ag vacancies is established between the surface of Ag oxide and the Ag_2O/Ag interface. Formation of the Ag_2O layer was confirmed by XRD, XPS, and TEM results (Figures 2 and 3). Recalling the well-known vacancy exchange-mediated ion diffusion theory, we propose that the exchange of positions between Ag vacancies and Ag ions causes diffusion of Ag ions from regions of the lower concentration of Ag vacancies (Ag_2O/Ag interface) to

https://doi.org/10.1021/acsomega.4c03608
ACS Omega 2024, 9, 28912–28925

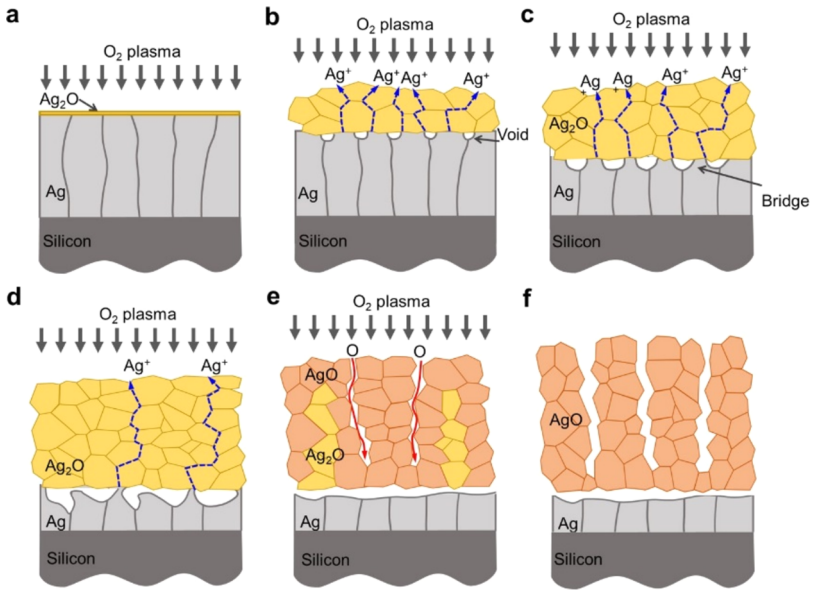

Figure 7. Schematic of the microstructural changes in thick Ag films during O_2 plasma treatment. (a, c) Oxide layer grows on the Ag film, accompanied by formation of Kirkendall voids. (d) The neighboring Kirkendall voids coalesce. (e, f) The upper oxide layer detaches from the remaining Ag film, and pores are formed within the oxide layer.

the higher concentration of Ag vacancies (the Ag_2O surface). A few smaller voids in the upper part of the Ag_2O layer may be caused by the coalescence of vacancies in the oxide, and this phenomenon has been commonly observed for thermal oxidation of metals.[42] Therefore, the proposed mechanism provides a satisfactory explanation for the previous argument[13,16] of enhanced outward diffusion of Ag ions, which was only deduced from observation of formation of voids at the Ag_2O/Ag interface. Based on this mechanism, the literature viewpoints—outward diffusion of Ag ions as the dominant transport process in the growing Ag_2O layer film, and the new Ag oxide is formed at the outermost surface of the existing oxide film—are thus put on a microscopic foundation.

Experimental results (Figures 2 and 3) show clearly that the growth of Ag oxide is accompanied by the generation of voids within the Ag_2O/Ag interfacial region; this is a clear signature of the nanoscale Kirkendall effect. This effect is a natural consequence of lasting outward diffusion of Ag atoms, as clarified above: as Ag atoms diffuse outward away from Ag films, vacancies left behind in the Ag lattice become supersaturated and coalesce into voids.[43−46] This phenomenon was already reported for plasma oxidation of Ag nanoparticles/nanowires.[13,16] We notice in a report[19] that formation of small voids along the Ag_2O/Ag interface seems to occur in plasma oxidation of Ag films under a rather complex plasma environment and elevated temperature, but its occurrence was somehow overlooked therein.[19]

It seems that some voids grow upward into the upper Ag_2O layer, as shown in the side-view SEM images (Figure 2a). We think this might be caused by artifacts induced by SEM cross section specimen preparation and image processing steps. On the one hand, the sample is fractured to facilitate SEM cross-sectional morphology characterization, and the fractured surface is not flat; on the other hand, it is rather challenging to extremely position the sample vertically against the sample stage to achieve accurate side-view SEM observation.

Interestingly, we found that Kirkendall voids seemed to be forming preferentially at the grain boundaries of Ag grains (Figure 5). It is known that atoms at grain boundaries are more energetic than atoms in the grain. It is reasonable that Ag atoms at grain boundaries prefer to diffuse outward; thus, supersaturation of lattice vacancies and formation of voids occur preferentially at grain boundaries.

(iii) Growth of the Ag_2O layer by oxidation of the Ag film until complete consumption of the Ag film (Figure 6d): After Kirkendall voids are formed within the interfacial region, outward diffusion of Ag atoms occurs at the Ag/oxide interface where the ligaments are in contact with the oxide layer. Unfortunately, there is no literature data about the rate of the jump of Ag atoms from the metal into the oxide layer. As plasma oxidation proceeds, Ag atoms continuously diffuse outward toward the Ag oxide surface (reaction front); thus, the Ag film becomes thinner; at the same time, more vacancies are left behind in the Ag lattices, vacancies coalesce, and thus Kirkendall voids grow. When Kirkendall voids reach the Si substrate, the walls of voids act as Ag bridges connecting the upper oxide layer and the Si substrate, resulting in still strong adhesion between the film and the Si substrate. Finally, these bridges are consumed, and the lower surface of the oxide layer reaches the Si substrate with complete conversion of the Ag film to Ag_2O. Although the interface between Ag_2O and Si looks smooth, the adhesion of the Ag_2O/Si interface is not as strong as that of the Ag/Si interface because the Ag film is directly deposited on the Si substrate.

(iv) The second stage of oxidation with conversion of Ag_2O to AgO: Formation of AgO and complete conversion of the Ag_2O film to the AgO film was confirmed by XRD, XPS, and TEM results (Figures 2 and 3). To the best of

https://doi.org/10.1021/acsomega.4c03608
ACS Omega 2024, 9, 28912−28925

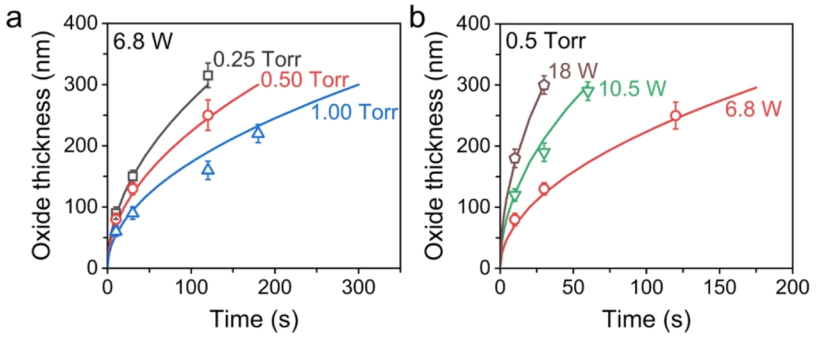

Figure 8. Parabolic rate law fitted for the growth of the oxide layer at the first stage of plasma oxidation of the 200 nm thick Ag film at different powers (a) and pressures (b).

our knowledge, the O_2 plasma oxidation behavior of the Ag_2O film and the important morphological and microstructural evolution during plasma oxidation were not reported before.

As proposed in the last section, we speculate that the creation of Ag vacancies can also occur at the surface of AgO during plasma exposure (eq 2). Similarly, a high concentration gradient of Ag vacancies was established between the surface of AgO oxide and the Ag_2O/AgO interface. The vacancy exchange-mediated ion diffusion theory causes diffusion of Ag ions from the Ag_2O/AgO interface to the AgO surface, and new AgO is formed at the outermost surface of the existing oxide film.

We propose that generation of pores through the oxide film is largely the outcome of the Kirkendall effect as described above, i.e., the coalescence of nanoscale Kirkendall voids generated within the oxides into large pores. It is possible that the difference between Ag and Ag_2O causes different distributions of coalesced voids in two stages: formation of large voids along the Ag_2O/Ag interface for the first stage of oxidation and formation of pores throughout oxides for the second stage. In a report,[19] formation of pores in oxides during plasma oxidation of Ag_2O to AgO (in a sputtering equipment) was also attributed to the outward diffusion of Ag ions and the Kirkendall effect. It is widely accepted that pore formation is caused by growth stress within the oxide layer.[47] We agree that stress owing to volume expansion during oxidation (larger volume AgO than Ag_2O and Ag) may play a certain role in formation of porous structures and the surface morphology at a larger scale (see Figure S4 in the Supporting Information). The relative contribution of the Kirkendall effect and stress will be an interesting future research topic.

With complete conversion of Ag_2O to AgO, the second stage of oxidation ends; prolonged exposure did not cause further changes in morphology and microstructures because of the discontinuation of oxidation reactions.

For thick Ag films, the partial oxidation behavior was identified with two distinguished distinct oxidation stages: the first stage is the same as that of thin films, i.e., oxidation of the Ag film to Ag_2O, and the second stage is conversion of Ag_2O to AgO but with the partial Ag film remaining unoxidized. Figure 7 illustrates the oxidation process of the thick Ag films.

(i) Figure 7a–c illustrates the first stage of oxidation, as observed in Figures 4 and 5. First, a very thin oxide layer is formed upon initial exposure to O_2 plasma. Second, the gradient of Ag vacancy-mediated outward diffusion of Ag ions from Ag/Ag_2O to the surface of Ag_2O induced growth of Ag_2O film, and the nanoscale Kirkendall effect induced the formation and growth of interfacial voids.

(ii) Figure 7d–f illustrates the second stage of oxidation. As oxidation progresses, unlike in the case of a thin film, the growth of the Ag_2O layer by oxidation of the Ag film does not completely consume the Ag film. Instead, further growth of the Ag_2O layer causes thinning of the Ag film accompanied by enlarged Kirkendall voids. When neighboring Kirkendall voids begin to coalesce (preferably at grain boundaries), the wall of coalesced voids, which act as Ag bridges connecting the upper oxide layer and the lower Ag film, becomes thinner, resulting in fewer and weak contacts between the oxide layer and the remaining Ag film. After most bridges are further consumed, they are broken, leading to seriously impeded transport of Ag atoms from the remaining Ag film to the upper Ag_2O layer.

The latter process of the second stage of oxidation is largely similar to that of the thin film, i.e., oxidation of Ag_2O to porous AgO. The end of this stage is again marked by complete conversion of the Ag_2O film. It is noteworthy that because adhesion between AgO and the remaining Ag film is very weak, detachment and wrinkling of the porous AgO layer is more pronounced due to growth stress in the oxide layer.

As shown in Figure S5, upon prolonged exposure to plasma (25 min), the upper AgO layer is seriously cracked, the remaining Ag film is not protected from plasma attack, and further oxidization occurs. The obtained structures resemble the final porous oxide structures observed for the thin Ag film.

Analyses of Growth Kinetics of Oxide Layers. The discussion above thus provides a full picture of morphology and microstructure evolution of Ag films during plasma oxidation, revealing the intricate interplay among atomic O, Ag ion diffusion, Kirkendall effect, and growth of oxide regulated by interfacial void coalescence. Insights gained from a mechanistic understanding of the plasma oxidation behavior of Ag films, together with quantitative measurements of the power/pressure/time dependence of oxide thickness, enable us to gain new insights into oxidation kinetics. Discussions will be given regarding a comparison of our results with literature results.

Based on eq 11, integration of the diffusion flux of Ag ions across the Ag_2O layer leads to the parabolic rate law

$$X_1^2 = k_1 t \tag{13}$$

https://doi.org/10.1021/acsomega.4c03608
ACS Omega 2024, 9, 28912–28925

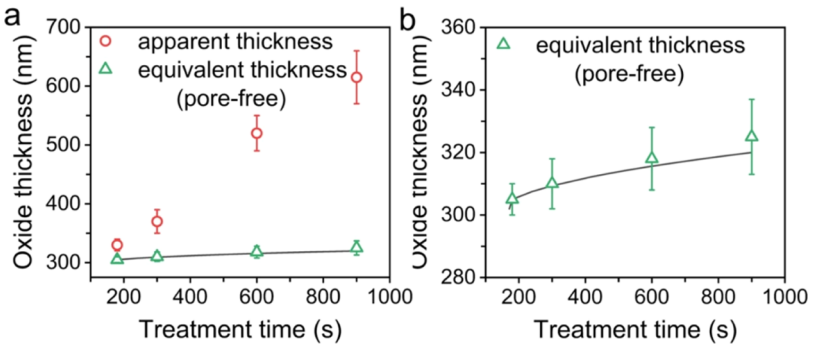

Figure 9. (a) Parabolic rate law fitted for the growth of the porous oxide film at the second stage of plasma oxidation at 6.8 W and 0.50 Torr for a 200 nm thick Ag film. Both data for the apparent thickness of the porous oxide film and the equivalent thickness of the dense film are shown. Curve fitting is given only for the equivalent thickness of the dense film. (b) The enlarged view.

where t is the time, k_1 is the rate constant, and $k_1 \propto -D_{Ag} + a(O)^{1/4}$. It can be seen that k_1 will increase with D_{Ag^+} and $a(O)$. Next, we will see that the power/pressure/time dependence of the thickness of the Ag_2O layer for the first stage of plasma oxidation of a 200 nm thick Ag film (also applicable to the first stage of oxidation of thicker Ag films) can be satisfactorily explained with the parabolic kinetics.

Experimental data give a good fit to parabolic kinetics, with an R-square of about 0.98. We found that different values of k_1 are obtained for different power/pressure values (Figure 8). At a fixed power of 6.8 W, k_1 decreases with increasing pressure from 7.5×10^{-12} cm^2/s at 0.25 Torr to 5.3×10^{-12} cm^2/s at 0.5 Torr and to 3.0×10^{-12} cm^2/s at 1.00 Torr. At a fixed pressure of 0.5 Torr, k_1 increases with increasing power from 5.3×10^{-12} cm^2/s at 6.8 W to 1.5×10^{-11} cm^2/s at 10.5 W and finally to 3.0×10^{-11} cm^2/s at 18 W. Therefore, the oxidation rate is larger at higher power and lower pressure. Calculations already show that the concentration of atomic O increases with power but decreases with pressure. Varied concentrations of atomic O cause the pressure/power dependence of the oxidation rate. To the best of our knowledge, it is for the first time that the pressure/power dependence of the oxidation rate of Ag films in plasma oxidation has been quantitatively determined.

The effect of the temperature rise during plasma oxidation needs to be discussed. The substrate temperature only rises slightly at 6.8 W to 310 K in 2 min and to 322 K in 15 min (Figure S3) and rises to 316 K in 2 min and 333 K in 15 min at 18 W. The effect of elevated substrate temperature during plasma oxidation for longer exposure and at higher power indeed desires more analysis; the estimation of the effect for the first stage of oxidation of the thin film is given here.

The diffusion coefficient of Ag ions can be calculated: $D_{Ag^+} \approx a^2 \nu \exp(-U/kT)$, where a is the interatomic distance, $\sim 3 \times 10^{-8}$ cm; ν is the atomic frequency of vibration, $\sim 10^{12}$ s^{-1}; T is the temperature, K; and U is the activation energy for diffusion of Ag ions, eV.[48] As reported, the energy for creating an Ag^+ vacancy is about 0.64 eV.[41] U is about half of the formation energy, ~0.32 eV.[48] D_{Ag^+} is about 5.7×10^{-9} cm^2/s at 310 K (6.8 W, 2 min) and 7.1×10^{-9} cm^2/s at 316 K (18 W, 2 min). It can be found that the effect of temperature rise is less than the effect of the power dependence of the concentration of atomic O.

Similarly, the analysis of oxidation kinetics of conversion from Ag_2O to AgO was carried out with consideration of the porous structures of oxides. Based on eq 12, the parabolic rate law can be obtained as follows

$$X_2^2 = k_2 t \tag{14}$$

where t is the time, X_2 is the thickness of the AgO layer, k_2 is the rate constant, and $k_2 \propto -D_{Ag^{2+}} a(O)^{1/3}$. It can be seen that k_2 will increase with $D_{Ag^{2+}}$ and $a(O)$. Because the diameter of pores is less than 100 nm, the Knudsen flow of the plasma species including atomic O into the pore is thus expected. It is hard to accurately calculate the $a(O)$ inside pores, but this information does not affect the discussion below because $a(O)$ inside pores should correlate positively with $a(O)$ in the chamber outside pores. Based on the parabolic kinetics, the power/pressure/time dependence of the thickness of the AgO layer for the second stage of plasma oxidation of the 200 nm thick Ag film as a typical system is explained. Considering porous structures of oxides in the second stage, in comparison to the dense Ag_2O in the first stage, we need to convert the apparent thickness of the oxide film to the equivalent thickness of pore-free dense oxide structures in order to use eq 13 to fit the experimental results.

The theoretical volume ratios of Ag_2O to Ag and AgO to Ag_2O are about 1.5 and 1.1, respectively. If the thickness of pristine Ag films is X_0, when Ag is completely oxidized to Ag_2O at the end of the first stage of plasma oxidation, the thickness of a dense Ag_2O film should be $1.5X_0$. During the oxidation of Ag_2O, the thickness of the AgO layer increases, $X_{AgO} = \sqrt{k_2 t}$, while the thickness of the Ag_2O film decreases, $X_{Ag_2O} = 1.5X_0 - \sqrt{k_2 t}/1.1$; thus, the total thickness of the dense Ag_2O/AgO film is $X_T = 1.5X_0 + 0.09\sqrt{k_2 t}$. Then, we will analyze our experimental results based on this equation. The solid thickness of the porous film can be obtained by $X_T = X_a(1-p)$, where p is the porosity and X_a is the apparent thickness of the porous Ag_2O/AgO film. Finally, k_2 is about 1.3×10^{-12} cm^2/s by fitting experimental data to the kinetics model (Figure 9).

In the past, it has been popularly assumed that diffusion of Ag ions across the oxide layer is driven by the concentration gradient of Ag ions, and the kinetic analyses were based on this assumption.[13,15] However, we already reveal that this assumption may be incorrect as described before that plasma oxidation of the Ag film is actually driven by the concentration gradient of Ag vacancy. Furthermore, in the literature, sometimes the apparent thickness of the oxide film was incorrectly used to fit the parabolic law, but the result may be problematic, since only the equivalent thickness of pore-free

https://doi.org/10.1021/acsomega.4c03608
ACS Omega 2024, 9, 28912−28925

dense oxide structures can be fitted physically using the parabolic law.

The quantitative analysis method of growth kinetics developed above thus provides a solid framework for future studies of plasma oxidation of metals.

CONCLUSIONS

Typical O_2 plasma oxidation behavior of Ag films with various thicknesses (100−400 nm) deposited on the Si substrate was studied at low plasma power (6.8−18 W) and moderate pressure (0.25−1.0 Torr) to facilitate observation and modeling of the full spectrum of morphology and microstructure evolution of Ag films and formed oxide films as well as oxidation kinetics.

Oxidation of thinner Ag films (thickness <200 nm) shows two-stage microstructural evolution. Oxidation is driven by the high concentration gradient of Ag vacancy with surface vacancies created through the reaction between atomic O and the incipient top oxide layer. In the first stage, a dense Ag_2O layer forms on the Ag film, accompanied by formation of Kirkendall voids at the Ag_2O/Ag interface. With increasing exposure time, the upper Ag_2O layer grows by consumption of the underlying Ag film, and Kirkendall voids enlarge until complete conversion of Ag to Ag_2O. In the second stage, the Ag_2O layer is further oxidized to AgO, and pores are formed via the Kirkendall effect until complete conversion of Ag_2O to AgO.

Thicker films (thickness >200 nm) feature partial oxidation and formation of a detached AgO film. Partial oxidation originates from the seriously impeded transport of Ag ions from the underlying Ag film to the upper oxide layer. Transport impediment is due to the significant coalescence of Kirkendall voids along the Ag_2O/Ag interface and the resulting breakage of bridges connecting the oxide layer and Ag film.

The growth kinetics of oxide layers/films is modeled with a parabolic law, which is derived by invoking the mechanism of atomic O-induced Ag vacancy creation and diffusion of Ag ions mediated via vacancy−Ag ion exchange. The plasma power/pressure dependence of the oxidation rate is thus rationalized by numerical calculation of the concentration of atomic O under different power/pressure values.

The findings reported and the methodology developed here contribute significantly to gaining deeper insights into the plasma oxidation behavior of Ag and other metals and will benefit fabrication of oxides with tailored microstructures.

ASSOCIATED CONTENT

Supporting Information

The Supporting Information is available free of charge at https://pubs.acs.org/doi/10.1021/acsomega.4c03608.

Additional SEM images; curve of substrate temperature with time under different powers; and calculation of the concentration of atomic O of O_2 plasma (PDF)

AUTHOR INFORMATION

Corresponding Authors

Dan Zhang − *School of Chemistry and Chemical Engineering and MIIT Key Laboratory of Critical Materials Technology for New Energy Conversion and Storage, School of Chemistry and Chemical Engineering, Harbin Institute of Technology, Harbin 150001, China*; Email: zhangd@hit.edu.cn

Yang Gan − *School of Chemistry and Chemical Engineering and MIIT Key Laboratory of Critical Materials Technology for New Energy Conversion and Storage, School of Chemistry and Chemical Engineering, Harbin Institute of Technology, Harbin 150001, China*; orcid.org/0000-0003-0358-2088; Email: ygan@hit.edu.cn

Author

ChengCheng Yuan − *School of Chemistry and Chemical Engineering and MIIT Key Laboratory of Critical Materials Technology for New Energy Conversion and Storage, School of Chemistry and Chemical Engineering, Harbin Institute of Technology, Harbin 150001, China*

Complete contact information is available at: https://pubs.acs.org/10.1021/acsomega.4c03608

Author Contributions

The manuscript was written through contributions of all authors. All authors have given approval to the final version of the manuscript.

Notes

The authors declare no competing financial interest.

ACKNOWLEDGMENTS

This project was sponsored by the Heilongjiang Touyan Team HITTY (Grant No. 20190033) and the National Key Laboratory of Science and Technology on Vacuum Electronics.

REFERENCES

(1) Dao, V. H.; Mapleback, B. J. Generation of Highly Porous Silver Nanowire Networks by Plasma Treatment and their Direct Application as Supercapacitor Electrodes. *Nanoscale* **2020**, *12* (22), 11868−11877.

(2) Wang, T.; Gu, S.; Fang, Y.; Zhang, D.; Xie, X.; Qu, Z.; Wang, Y.; Zhao, X.; Wu, J.; Lee, C. C.; Huo, Y. Plasma-induced growth mechanism of surface-state silver oxide in nanoscale for low-temperature bonding technology. *Mater. Charact.* **2023**, *199*, No. 112830.

(3) Ooi, C.; Goh, G. K. L. Formation of cuprous oxide films via oxygen plasma. *Thin Solid Films* **2010**, *518* (24), E98−E100.

(4) Li, Y.; Hess, D. W. Transport Considerations in the Plasma-Assisted Oxidation of Copper Films. *J. Electrochem. Soc.* **2004**, *151* (1), No. G40.

(5) Moon, J.; Kim, Y. H.; Chung, C. H.; Lee, S. J.; Park, D. J.; Song, Y. H. Growth of thin Si oxide in a cyclic oxygen plasma environment below 200 °C. *Appl. Surf. Sci.* **2008**, *254* (20), 6422−6427.

(6) Klages, C. P.; Jung, A.; Betz, M. L.; Raev, V. Low-Temperature Plasma Oxidation of Aluminum by Ar-O_2 Mixtures in a Dielectric-Barrier Discharge Reactor. *Plasma Chem. Plasma Process.* **2023**, *43* (5), 933−955.

(7) Varghese, B.; Reddy, M. V.; Yanwu, Z.; Lit, C. S.; Hoong, T. C.; Rao, G. V. S.; Chowdari, B. V. R.; Wee, A. T. S.; Lim, C. T.; Sow, C. H. Fabrication of NiO Nanowall Electrodes for High Performance Lithium Ion Battery. *Chem. Mater.* **2008**, *20* (10), 3360−3367.

(8) Bhan, M. K.; Nag, P. K.; Miller, G. P.; Gregory, J. C. Chemical and morphological changes on silver surfaces produced by microwave generated atomic oxygen. *J. Vae. Sci. Technol. A* **1994**, *12* (3), 699−706.

(9) Li, L.; Yang, J. C.; Minton, T. K. Morphological Changes at a Silver Surface Resulting from Exposure to Hyperthermal Atomic Oxygen. *J. Phys. Chem. C* **2007**, *111* (18), 6763−6771.

(10) Edwards, D. L.; Williams, J. R.; Fromhold, A. T.; Barnes, P. A.; et al. The oxidation of polycrystalline silver films by thermal, ground-state atomic oxygen. *Nucl. Instrum. Methods Phys. Res., Sect. B* **1993**, *79*, 676−679.

(11) Rooij, A. The Oxidation of Silver by Atomic Oxygen. *ESA J.* **1989**, *13*, 363−382.
(12) El Mel, A. A.; Stephant, N.; Hamon, J.; Thiry, D.; Chauvin, A.; Chettab, M.; Gautron, E.; Konstantinidis, S.; Graniera, A.; Tessiera, P. Y. Creating nanoporosity in silver nanocolumns by direct exposure to radio-frequency air plasma. *Nanoscale* **2016**, *8* (1), 141−148.
(13) El Mel, A. A.; Stephant, N.; Molina-Luna, L.; Gautron, E.; Haik, Y.; Tabet, N.; Tessier, P. Y.; Gautier, R. Kirkendall Effect vs Corrosion of Silver Nanocrystals by Atomic Oxygen: From Solid Metal Silver to Nanoporous Silver Oxide. *J. Phys. Chem. C* **2017**, *121* (35), 19497−19504.
(14) El Mel, A. A.; Mansour, S. A.; Pasha, M.; Zekri, A.; Ponraj, J.; Shetty, A.; Haik, Y. Oxidation of Au/Ag films by oxygen plasma: phase separation and generation of nanoporosity. *Beilstein J. Nanotechnol.* **2020**, *11*, 1608−1614.
(15) Xu, W.; Li, C. X.; Zhang, Q. Y.; Ma, C. Y.; Wang, Q.; Wen, D. H.; Li, L. Formation of hierarchical porosity in oxidation of Ag films by reactive sputtering deposition of metal oxides via the Kirkendall effect. *Nanoscale* **2019**, *11* (20), 10034−10044.
(16) Li, Y.; Zhang, Y.; Fu, H.; Wang, Z.; Li, X. Plasma-assisted speedy synthesis of mesporous Ag_2O nanotube. *Mater. Lett.* **2014**, *126*, 131−134.
(17) Ma, C.; Trujillo, M. J.; Camden, J. P. Nanoporous Silver Film Fabricated by Oxygen Plasma: A Facile Approach for SERS Substrates. *ACS Appl. Mater. Interfaces* **2016**, *8* (36), 23978−23984.
(18) Xu, W.; Wang, S. Q.; Zhang, Q. Y.; Ma, C. Y.; Li, X. N.; Wang, Q.; Wen, D. H. Abnormal Oxidation of Ag Films and Its Application to Fabrication of Photocatalytic Films with a-TiO2/h-Ag2O Heterostructure. *J. Phys. Chem. C* **2017**, *121* (18), 9901−9909.
(19) Xu, W.; Tang, H.; Zhou, N.; Zhang, Q. Y.; Peng, B.; Shen, Y. Enhanced photocatalytic activity of TiO_2/Ag_2O heterostructures by optimizing the separation of electric charges. *Vacuum* **2021**, *190* (2), No. 110283.
(20) Xu, W.; Wang, S. Q.; Zhang, Q. Y.; Ma, C. Y.; Wang, Q.; Wen, D. H.; Li, X. N. Hierarchically structured AgO films with nanoporosity for photocatalyst and all solid-state thin film battery. *J. Alloys Compd.* **2019**, *802*, 210−216.
(21) Kern, W.; Puotinen, D. A. Cleaning solutions based on hydrogen peroxide for use in silicon semiconductor technology. *RCA Rev.* **1970**, *31*, 187−206.
(22) Stuckner, J.; Frei, K.; McCue, I.; Demkowicz, M. J.; Murayama, M. AQUAMI: An open source Python package and GUI for the automatic quantitative analysis of morphologically complex multiphase materials. *Comput. Mater. Sci.* **2017**, *139*, 320−329.
(23) Krishna, D. N. G.; Philip, J. Review on surface-characterization applications of X-ray photoelectron spectroscopy (XPS): Recent developments and challenges. *Appl. Surf. Sci. Adv.* **2022**, *12*, No. 100332.
(24) Gunter, P. L. J.; Gijzeman, O. L. J.; Niemantsverdriet, J. W. Surface roughness effects in quantitative XPS: magic angle for determining overlayer thickness. *Appl. Surf. Sci.* **1997**, *115*, 342−346.
(25) Lee, C.; Lieberman, M. A. Global model of Ar, O_2, Cl_2, and Ar/O_2 high density plasma discharges. *J. Vac. Sci. Technol. A* **1995**, *13* (2), 368−380.
(26) Lee, C.; Graves, D. B.; Lieberman, M. A.; Hess, D. W. Global Model of Plasma Chemistry in a High Density Oxygen Discharge. *J. Electrochem. Soc.* **1994**, *141* (6), 1546−1555.
(27) Dai, X. J. Kinetic Model of an RF Discharge in Oxygen. *Aust. J. Phys.* **1996**, *49* (6), 1169−1180.
(28) Hu, Y. Z.; Wang, Y. Q.; Li, M.; Joseph, J.; Irene, E. A. In situ investigation of temperature and bias dependent effects on the oxide growth of Si and Ge in an electron cyclotron resonance. *J. Vac. Sci. Technol. A* **1993**, *11* (4), 900−904.
(29) Dai, X. J.; Hamberger, S. M.; Bean, R. A. Reactive plasma Species in the Modification of Wool Fiber. *Aust. J. Phys.* **1995**, *48*, 939−951.
(30) Mozetic, M.; Cvelbar, U. Determination of the neutral oxygen atom density in a plasma reactor loaded with metal samples. *Plasma Sources Sci. Technol.* **2009**, *18* (3), No. 034002.
(31) Kaspar, T. C.; Droubay, T. C.; Chambers, S. A. Atomic oxygen flux determined by mixed-phase Ag/Ag_2O deposition. *Thin Solid Films* **2010**, *519* (2), 635−640.
(32) Montemore, M. M.; Van Spronsen, M. A.; Madix, R. J.; Friend, C. M. O_2 Activation by Metal Surfaces: Implications for Bonding and Reactivity on Heterogeneous Catalysts. *Chem. Rev.* **2018**, *118* (5), 2816−2862.
(33) Boas, C. R. S. V.; Sturm, J. M.; van den Beld, W. T. E.; Bijkerk, F. Oxidation kinetics of transition metals exposed to molecular and atomic oxygen. *Materialia* **2021**, *20*, No. 101203.
(34) Cai, W.; Zhong, H.; Zhang, L. Optical measurements of oxidation behavior of silver nanometer particle within pores of silica host. *J. Appl. Phys.* **1998**, *83* (3), 1705−1710.
(35) Rooij, A. The Oxidation of Silver by Atomic Oxygen. *ESA J.* **1989**, *13* (4), 363−382.
(36) Fehlner, F. P.; Mott, N. F. Low-Temperature Oxidation. *Oxid. Met.* **1970**, *2* (1), 59−99.
(37) Nakamura, R.; Lee, J. G.; Tokozakura, D.; Mori, H.; Nakajima, H. Formation of hollow ZnO through low-temperature oxidation of Zn nanoparticles. *Mater. Lett.* **2007**, *61* (4−5), 1060−1063.
(38) Ren, Y.; Chim, W. K.; Chiam, S. Y.; Huang, J.; Pi, C.; Pan, J. Formation of Nickel Oxide Nanotubes with Uniform Wall Thickness by Low-Temperature Thermal Oxidation Through Understanding the Limiting Effect of Vacancy Diffusion and the Kirkendall Phenomenon. *Adv. Funct. Mater.* **2010**, *20* (19), 3336−3342.
(39) Nakamura, R.; Tokozakura, D.; Nakajima, H.; Lee, J. G.; Mori, H. Hollow oxide formation by oxidation of Al and Cu nanoparticles. *J. Appl. Phys.* **2007**, *101* (7), No. 074303.
(40) Park, B. I.; Park, J. S.; Yu, S.; Cho, S. H.; Byun, J. Y.; Oh, J.; Lee, S. Y. Hollow/porous-walled SnO_2 via nanoscale Kirkendall diffusion with irregular particles. *Acta Mater.* **2020**, *186*, 20−28.
(41) Talukdar, M. I.; Baker, E. H. Conductivity Studies On Silver Oxide. *Solid State Commun.* **1969**, *7* (2), 309−310.
(42) Hauffe, K. The Mechanism of Oxidation of Metals—Theory. In *Oxidation of Metals*; Springer: Boston, MA, 1965.
(43) Yin, Y.; Rioux, R. M.; Erdonmez, C. K.; Hughes, S.; Somorjai, G. A.; Alivisatos, A. P. Formation of Hollow Nanocrystals Through the Nanoscale Kirkendall Effect. *Science* **2004**, *304* (5671), 711−714.
(44) Cabot, A.; Puntes, V. F.; Shevchenko, E.; Yin, Y.; Balcells, L.; Marcus, M. A.; Hughes, S. M.; Alivisatos, A. P. Vacancy Coalescence during Oxidation of Iron Nanoparticles. *J. Am. Chem. Soc.* **2007**, *129* (34), 10358−10360.
(45) Yin, Y.; Erdonmez, C. K.; Cabot, A.; Hughes, S.; Alivisatos, A. P. Colloidal Synthesis of Hollow Cobalt Sulfide Nanocrystals. *Adv. Funct. Mater.* **2006**, *16* (11), 1389−1399.
(46) Wang, W. S.; Dahl, M.; Yin, Y. D. Hollow Nanocrystals through the Nanoscale Kirkendall Effect. *Chem. Mater.* **2013**, *25* (8), 1179−1189.
(47) Shen, P. Z.; Song, M.; Gao, H. Y.; He, Y. H.; Zou, J.; Xu, N. P.; Huang, B. Y.; Liu, C. T. Structural characteristics and high-temperature oxidation behavior of porous Fe−40 at.%Al alloy. *J. Mater. Sci.* **2009**, *44* (16), 4413−4421.
(48) Cabrera, N.; Mott, N. F. Theory of the oxidation of metals. *Rep. Prog. Phys.* **1949**, *12*, 163−184.

https://doi.org/10.1021/acsomega.4c03608
ACS Omega 2024, 9, 28912−28925